Supporting Information

Conjugated Backbone Optimization of All-Fused-Ring Acceptor for Efficient and Stable Organic Solar Cells

Jun Feng,[a] Yue Liu,[a] Hang Yang,[a] Kewei Hu,[a] Xinyu Jiang,[a] Naizhe Cui,[a] Yue Wu,[a] and Chaohua Cui[a,b,*]

[a] *Laboratory of Advanced Optoelectronic Materials, Suzhou Key Laboratory of Novel Semiconductor-Optoelectronics Materials and Devices, College of Chemistry Chemical Engineering and Materials Science, Soochow University, Suzhou 215123, China*

[b] *Jiangsu Key Laboratory of Advanced Negative Carbon Technologies, Soochow University, Suzhou 215123, Jiangsu, PR China*

E-mail: cuichaohua@suda.edu.cn

Experimental details

1. Materials synthesis

All chemicals and solvents were reagent grade, purchased from Aladdin or Energy Chemical, and used without further purification. The polymer donor PTQ10 was synthesized according to methods reported in the literature.[1] **Compounds 2a** and **2b** were synthesized according to methods reported in the literature.[2] Schemes S1-S3 show the synthetic routes of **DPT-T**, **DPT-TT**, and **DPP-T**, and the detailed synthesis procedures are described below. Tetrahydrofuran was dried using sodium before use.

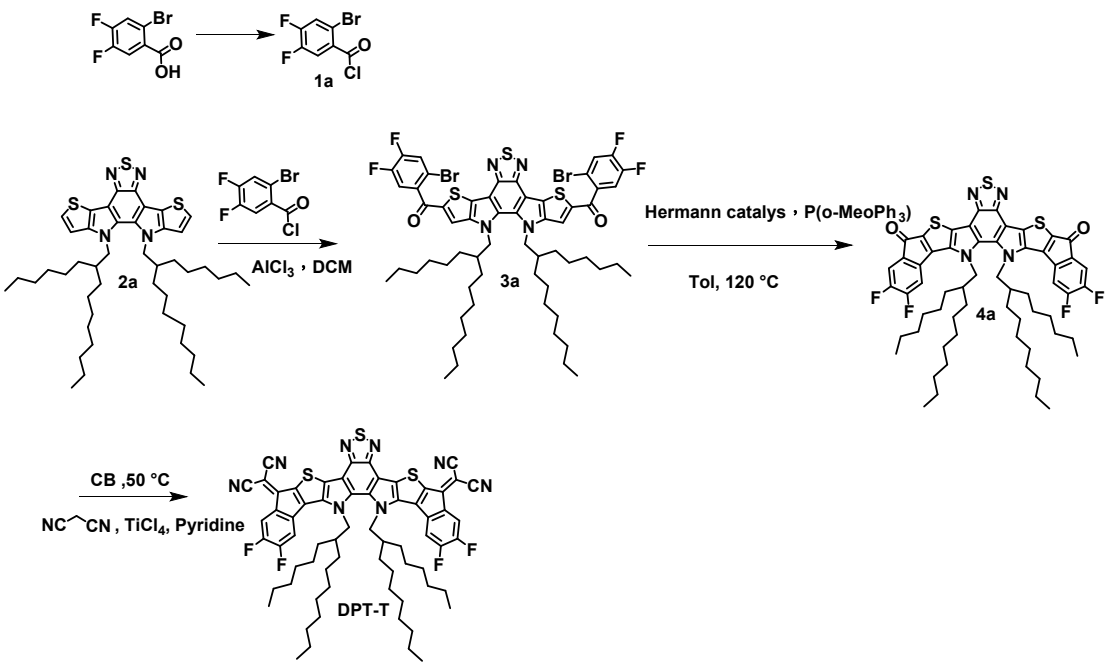

Scheme S1. Synthetic routes of DPT-T.

Compound 1a: To a solution of 2-bromo-4,5-difluorobenzoic acid (500 mg, 2.110 mmol) in DCM (8 mL), oxalyl chloride (347.5 mg, 2.738 mmol) was added, and then the mixture was stirred at 0 °C for 4 h. the reaction was directly spin-dried without further processing and used directly in the next step.

Compound 3a: Under the protection of argon, compound **1a** (539 mg, 2.110 mmol) and aluminum chloride (280 mg, 2.100 mmol) were added to a solution of compound **2a** (500 mg, 0.645 mmol) in anhydrous dichloromethane. The mixture was stirred at room temperature overnight. Then, the solution was quenched with water and extracted with CH_2Cl_2. The organic layer was washed with water and brine and dried over $MgSO_4$. After removal of the solvent, this crude product was purified by silica gel chromatography (petroleum ether/dichloromethane = 1.5:1.0, v/v) to afford compound **3a** as an orange-red solid (541 mg, 0.446 mmol, yield: 69%). ^{1}H NMR (400 MHz, Chloroform-*d*) δ 7.67 – 7.51 (m, 4H), 7.41 (dd, *J* = 9.4, 7.8 Hz, 2H), 4.48 (d, *J* = 7.7 Hz, 4H), 1.97 (h, *J* = 6.7 Hz, 2H), 0.84 (s, 60H). ^{13}C NMR (101 MHz, $CDCl_3$) δ 185.56, 152.40, 150.60, 149.71, 148.21, 147.38, 145.08, 142.63, 137.11, 134.80, 129.60, 122.78, 122.58, 119.38, 118.15, 117.96, 114.09, 112.30, 54.74, 38.32, 31.77, 31.53, 30.54, 29.57, 29.13, 25.61, 22.59, 22.47, 14.08, 13.98. MALDI-TOF

MS: calcd. for $C_{60}H_{72}Br_2F_4N_4O_2S_3$ m/z = 1213.24; found 1212.467.

Compound 4a: Under the protection of argon, Herrmann catalyst (transbis(acetato)bis[o-(di-o-tolylphosphino)benzyl]dipalladium (II)) (3 mg, 0.003 mmol), P(*o*-MeOPh)$_3$ (2 mg, 0.006 mmol), pivalic acid (18 mg, 0.176 mmol), and Cs_2CO_3 (160 mg, 0.491 mmol) were added to a solution of compound **3a** (216 mg, 0.178 mmol) in 10 mL toluene. The mixture was heated to 120 °C and stirred for 32 h. Then, with the removal of solvent, this crude product was purified by silica gel chromatography (petroleum ether/dichloromethane = 1.0:1.5, v/v) to afford compound **4a** as a purple solid (168 mg, 0.160 mmol, yield: 90%). ^{1}H NMR (400 MHz, Chloroform-*d*) δ 7.43 (td, *J* = 7.9, 2.7 Hz, 2H), 7.18 (dd, *J* = 9.3, 6.2 Hz, 2H), 4.62 (d, *J* = 7.7 Hz, 4H), 1.96 (s, 2H), 1.45 – 0.23 (m, 60H). ^{13}C NMR (151 MHz, cdcl$_3$) δ 182.64, 153.77, 152.16, 151.09, 149.49, 147.04, 139.46, 139.27, 137.54, 136.15, 136.06, 135.04, 134.84, 114.83, 114.70, 112.94, 110.78, 110.64, 55.51, 39.25, 31.71, 31.49, 29.29, 29.07, 26.70, 23.98, 22.56, 22.42, 14.04, 13.90. MALDI-TOF MS: calcd. for $C_{60}H_{70}F_4N_4O_2S_3$ m/z = 1051.42; found 1050.113.

Compound DPT-T: To a stirred solution of compound **4a** (150 mg, 0.142 mmol) and malononitrile (46.9 mg, 0.710 mmol) in 15 mL chlorobenzene was added 0.3 mL pyridine and 0.3 mL $TiCl_4$, and the solution was heated to 50 °C for 4 h. Then, the solution was poured into water and extracted with CH_2Cl_2, and the organic layer was washed with water and brine and dried over $MgSO_4$. After removal of the solvent, this crude product was purified by silica gel chromatography (petroleum ether/dichloromethane = 1.0:1.0, v/v) to afford **DPT-T** as a black solid (114 mg, 0.099 mmol, yield: 70%). ^{1}H NMR (400 MHz, Chloroform-*d*) δ 8.15 (dd, J = 9.8, 7.1 Hz, 2H), 7.29 (dd, J = 9.3, 6.8 Hz, 2H), 4.60 (s, 4H), 1.90 (s, 2H), 1.35 – 0.51 (m, 60H). ^{13}C NMR (151 MHz, cdcl$_3$) δ 154.31, 153.70, 151.99, 150.64, 149.06, 146.70, 138.66, 137.98, 137.75, 136.84, 135.40, 134.63, 133.76, 117.23, 117.09, 113.65, 113.40, 112.76, 111.62, 111.48, 72.20, 55.99, 39.37, 31.76, 31.49, 29.90, 29.34, 29.16, 26.97, 24.29, 22.61, 14.08, 13.92. MALDI-TOF MS: calcd. for $C_{66}H_{70}F_4N_8S_3$ m/z =

1147.52; found 1145.985.

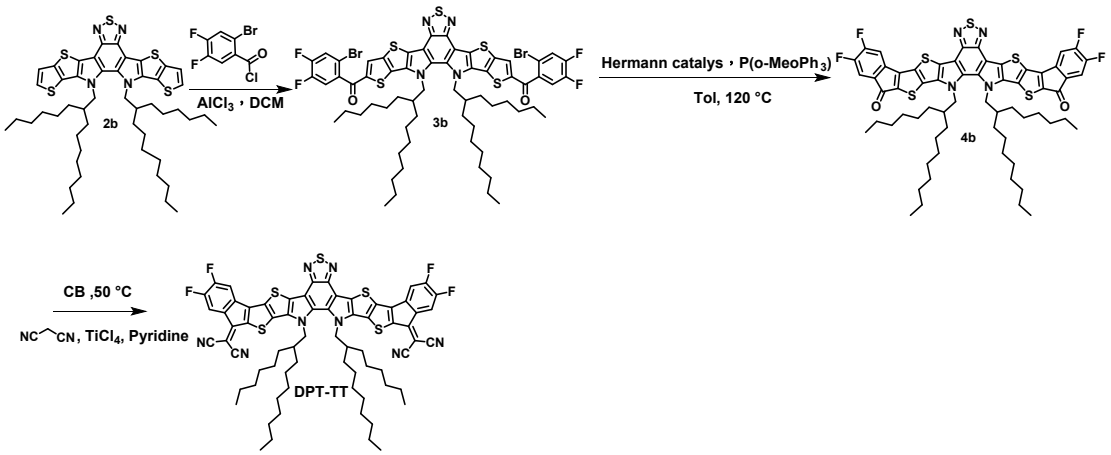

Scheme S2. Synthetic routes of DPT-TT.

Compound 3b: Under the protection of argon, **1a** (539 mg, 2.110 mmol) and aluminum chloride (280 mg, 2.100 mmol) were added to a solution of compound **2b** (621.2 mg, 0.700 mmol) in anhydrous dichloromethane. The mixture was stirred at room temperature overnight. Then, the solution was quenched with water and extracted with CH_2Cl_2. The organic layer was washed with water and brine and dried over anhydrous $MgSO_4$. After the removal of solvent, the crude product was purified by silica gel chromatography (petroleum ether/dichloromethane = 1.5:1.0, v/v) to afford compound **3b** as an orange-red solid (696 mg, 0.525 mmol, yield: 75%). ^{1}H NMR (400 MHz, Chloroform-*d*) δ 7.72 (s, 2H), 7.58 (dd, *J* = 9.4, 6.9 Hz, 2H), 7.41 (dd, *J* = 9.4, 7.8 Hz, 2H), 4.68 (d, *J* = 7.8 Hz, 4H), 2.11 – 2.00 (m, 2H), 1.21 – 0.66 (m, 60H). ^{13}C NMR (101 MHz, $CDCl_3$) δ 185.29, 152.33, 150.63, 149.76, 148.24, 141.75, 141.56, 136.65, 133.20, 131.90, 130.64, 128.89, 122.93, 122.73, 118.15, 117.95, 114.15, 112.65, 55.31, 38.96, 31.75, 31.54, 30.37, 29.67, 29.34, 29.31, 29.14, 25.43, 22.59, 22.49, 14.11, 13.98. MALDI-TOF MS: calcd. for $C_{64}H_{72}Br_2F_4N_4O_2S_5$ m/z = 1325.41; found 1323.732.

Compound 4b: Under the protection of argon, Herrmann catalyst transbis(acetato)bis[*o*-(di-*o*-tolylphosphino)benzyl]dipalladium (II)) (3 mg, 0.003

mmol), P(*o*-MeOPh)$_3$ (2 mg, 0.006 mmol), pivalic acid (18 mg, 0.176 mmol), and Cs_2CO_3 (160 mg, 0.491 mmol) were added to a solution of compound **3b** (237 mg, 0.179 mmol) in 10.0 mL toluene. The mixture was heated to 120 °C and stirred for 32 hours. Then, with the removal of solvent, this crude product was purified by silica gel chromatography (petroleum ether/dichloromethane = 1.0:1.5, v/v) to afford compound **4b** as a purple solid (191 mg, 0.164 mmol, yield: 92%). ^{1}H NMR (400 MHz, Chloroform-*d*) δ 7.39 (dd, *J* = 8.4, 7.0 Hz, 2H), 7.11 (dd, *J* = 8.6, 6.3 Hz, 2H), 4.64 (d, *J* = 7.8 Hz, 4H), 2.13 – 2.00 (m, *J* = 6.5 Hz, 2H), 1.28 – 0.65 (m, 60H). ^{13}C NMR (151 MHz, cdcl$_3$) δ 182.32, 154.04, 152.34, 151.53, 149.76, 148.87, 147.23, 136.58, 135.83, 135.36, 134.75, 134.39, 133.41, 133.13, 128.63, 114.38, 112.84, 110.46, 55.48, 39.04, 31.78, 31.53, 30.43, 30.35, 29.70, 29.37, 29.18, 25.48, 22.59, 22.47, 14.05, 13.94. MALDI-TOF MS: calcd. for $C_{64}H_{70}F_4N_4O_2S_5$ m/z = 1163.58; found 1161.913.

Compound DPT-TT: To a stirred solution of compound **4b** (180 mg, 0.154 mmol) and malononitrile (51 mg, 0.772 mmol) in 15 mL chlorobenzene was added 0.3 mL pyridine and 0.3 mL $TiCl_4$, and then the solution was heated to 50 °C for 4 h. Then, the solution was poured into water and extracted with CH_2Cl_2, and the organic layer was washed with water and brine and dried over $MgSO_4$. After the removal of solvent, this crude product was purified by silica gel chromatography (petroleum ether/dichloromethane = 1.0:1.0, v/v) to afford **DPT-TT** as a black solid (155 mg, 0.123 mmol, yield: 80%). ^{1}H NMR (400 MHz, Chloroform-*d*) δ 8.10 (dd, J = 9.8, 6.9 Hz, 2H), 7.28 (s, 1H), 7.24 (s, 1H), 4.63 (d, J = 7.9 Hz, 4H), 2.04 (d, J = 5.1 Hz, 2H), 1.45 – 0.80 (m, 60H). ^{13}C NMR (151 MHz, cdcl$_3$) δ 154.78, 153.76, 152.04, 150.95, 149.37, 147.19, 144.76, 137.17, 136.79, 134.82, 134.27, 134.05, 133.65, 129.82, 116.94, 116.80, 113.70, 113.49, 112.68, 111.27, 111.14, 71.81, 55.74, 39.13, 31.78, 31.49, 30.49, 29.67, 29.32, 29.18, 25.60, 22.60, 22.47, 14.07, 13.94. MALDI-TOF MS: calcd. for $C_{70}H_{70}F_4N_8S_5$ m/z = 1259.68; found 1257.904.

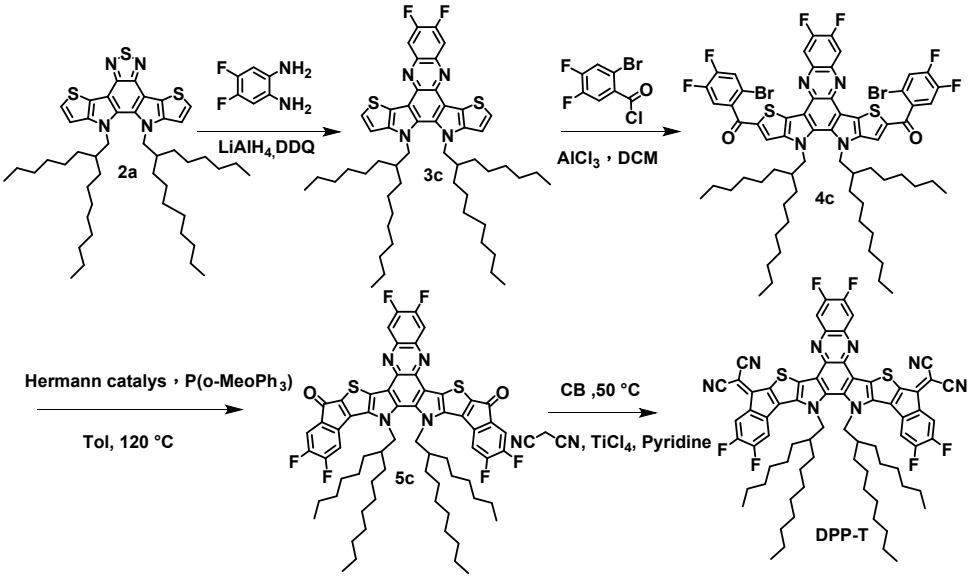

Scheme S3. Synthetic routes of DPP-T.

Compound 3c: Under the protection of argon, $LiAlH_4$ (293.7 mg, 7.740 mmol) was added to a solution of compound **2a** (600 mg, 0.774 mmol) in tetrahydrofuran (THF, 15 mL). The resulting mixture was stirred and heated to 82 °C and then refluxed overnight. After being cooled to 0 °C, water (35 mL) was slowly dropped into the mixture and extracted with dichloromethane. The organic layer was dried over anhydrous $MgSO_4$ for 5 min. After removing the solvent, the crude product was dissolved in chloroform (20 mL), and then 3-dichloro-5,6-dicyano-1,4-benzoquinone (DDQ) (202.06 mg, 0.890 mmol) and 1,2-diaminobenzene (536 mg, 3.719 mmol) were added to the solution in turn. The reaction was stirred at room temperature for 6 h, and the solvent was removed under vacuum. Finally, the residue was purified by silica gel chromatography (petroleum ether/dichloromethane = 4:1, v/v) to afford compound **3c** (530 mg, 0.620 mmol, yield: 80%) as an orange-red solid. ^{1}H NMR (400 MHz, Chloroform-*d*) δ 8.13 (t, *J* = 9.7 Hz, 2H), 7.48 (d, *J* = 5.2 Hz, 2H), 7.19 (d, *J* = 5.2 Hz, 2H), 4.54 (d, *J* = 7.8 Hz, 4H), 2.08 (p, *J* = 6.9 Hz, 2H), 1.20 – 0.68 (m, 60H). ^{13}C NMR (101 MHz, $CDCl_3$) δ 152.76, 150.18, 145.16, 138.35, 138.07, 132.76, 127.17, 121.56, 115.99, 114.22, 114.16, 111.73, 54.46, 38.16, 31.78, 31.58, 30.62, 29.63, 29.33, 29.31, 29.14, 25.66, 22.59, 22.47, 14.07, 13.97. MALDI-TOF MS: calcd. for $C_{52}H_{72}F_2N_4S_2$ m/z = 855.29; found 854.631.

Compound 4c: Under the protection of argon, **1a** (430 mg, 1.683 mmol) and aluminum chloride (224.7 mg, 1.685 mmol) were added to a solution of compound **3c** (480 mg, 0.561 mmol) in anhydrous dichloromethane. The mixture was stirred at room temperature overnight. Then, the solution was quenched with water and extracted with CH_2Cl_2. The organic layer was washed with water and brine and dried over $MgSO_4$. After the removal of the solvent, this crude product was purified by silica gel chromatography (petroleum ether/dichloromethane = 1.5:1.0, v/v) to afford compound **4c** (523 mg, 0.404 mmol, yield: 72%) as an orange-red solid. ^{1}H NMR (400 MHz, Chloroform-*d*) δ 8.13 (t, *J* = 9.4 Hz, 2H), 7.67 – 7.54 (m, 4H), 7.43 (dd, *J* = 9.4, 7.8 Hz, 2H), 4.51 (d, *J* = 7.8 Hz, 4H), 2.04 (q, *J* = 6.7 Hz, 2H), 1.18 – 0.67 (m, 60H). ^{13}C NMR (101 MHz, $CDCl_3$) δ 185.83, 145.12, 143.09, 139.13, 139.07, 138.00, 137.24, 134.57, 130.04, 129.93, 122.82, 122.62, 119.09, 118.17, 117.97, 117.58, 114.32, 114.05, 54.74, 38.46, 31.75, 31.54, 30.65, 30.58, 29.59, 29.28, 29.27, 29.13, 25.67, 22.56, 22.47, 14.04, 13.96. MALDI-TOF MS: calcd. for $C_{66}H_{74}Br_2F_6N_4O_2S_2$ m/z = 1293.26; found 1292.547.

Compound 5c: Under the protection of argon, Herrmann catalyst transbis(acetato)bis[o-(di-o-tolylphosphino)benzyl]dipalladium (II)) (4 mg, 0.004 mmol), P(*o*-MeOPh)$_3$ (2.67 mg, 0.008mmol), pivalic acid (23 mg, 0.225 mmol), and Cs_2CO_3 (202 mg, 0.620 mmol) were added to a solution of compound **4c** (293 mg, 0.227 mmol) in 10 mL toluene. The mixture was heated to 120 °C and stirred for 32 h. Then, with the removal of solvent, this crude product was purified by silica gel chromatography (petroleum ether/dichloromethane = 1.0:1.5, v/v) to afford compound **5c** (210 mg, 0.186 mmol, yield: 82%) as a purple solid. ^{1}H NMR (400 MHz, Chloroform-*d*) δ 8.00 (t, J = 9.4 Hz, 2H), 7.37 (dd, J = 8.3, 7.3 Hz, 2H), 7.11 (dd, J = 9.3, 6.2 Hz, 2H), 4.60 (d, J = 7.8 Hz, 4H), 1.96 (d, J = 11.2 Hz, 2H), 0.93 (dd, J = 175.5, 30.1 Hz, 60H). ^{13}C NMR (151 MHz, $cdcl_3$) δ 182.76, 153.82, 152.12, 151.12, 149.35, 139.94, 139.22, 138.44, 137.54, 137.42, 136.60, 136.31, 134.98, 118.07, 114.65, 114.52, 113.92, 110.73, 110.59, 55.87, 39.37, 31.69, 31.52, 31.13, 29.69, 29.31, 29.09, 26.63, 24.60, 22.53, 22.44, 13.99, 13.87. MALDI-TOF MS: calcd. for

$C_{66}H_{72}F_4N_4O_2S_2$ m/z = 1131.44; found 1130.028.

Compound DPP-T: To a stirred solution of compound **5c** (200 mg, 0.177 mmol) and malononitrile (59 mg, 0.893 mmol) in 15 mL chlorobenzene was added 0.3 mL pyridine and 0.3 mL $TiCl_4$, and the solution was heated to 50 °C for 4 h. Then, the solution was poured into water and extracted with CH_2Cl_2, and the organic layer was washed with water and brine and dried over $MgSO_4$. After the removal of solvent, this crude product was purified by silica gel chromatography (petroleum ether/dichloromethane = 1.0:1.0, v/v) to afford **DPP-T** as a black solid (152 mg, 0.124 mmol, yield: 70%). ^{1}H NMR (400 MHz, Chloroform-*d*) δ 8.12 (d, J = 2.9 Hz, 2H), 8.11 – 8.07 (m, 2H), 7.25 – 7.20 (m, 2H), 4.57 (d, J = 7.3 Hz, 4H), 1.89 (s, 2H), 0.93 (dd, J = 181.1, 37.5 Hz, 60H). ^{13}C NMR (151 MHz, cdcl$_3$) δ 154.58, 153.62, 151.91, 150.65, 148.89, 139.65, 139.26, 138.89, 137.71, 137.44, 136.92, 135.31, 134.87, 133.83, 119.01, 117.26, 117.11, 114.57, 114.48, 113.55, 112.96, 111.43, 111.29, 72.07, 55.92, 39.40, 31.72, 31.49, 29.44, 29.31, 29.11, 26.89, 24.40, 22.54, 14.01, 13.87. MALDI-TOF MS: calcd. for $C_{72}H_{72}F_6N_8S_2$ m/z = 1227.53; found 1226.015.

2. Instruments and general methods

NMR measurements.

NMR spectra were recorded in $CDCl_3$ on a Bruker AV 400 MHz FT-NM spectrometer, and chemical shifts are quoted relative to tetramethylsilane for 1H and ^{13}C nuclei. The ^{1}H and ^{13}C spectra of the target molecules are shown in Figure S20-S25.

MALDI-TOF measurements.

The molecular mass was confirmed by using an Ultraflextreme matrix-assisted laser desorption ionization mass spectrometer (MALDI-TOF-MS). The spectra of the target molecules are shown in Figure S26-S28.

Optical characterizations.

UV–vis absorption spectra were recorded on a Cary 5000 UV–vis-NIR Spectrophotometer. For the solid-state measurements, two small-molecule solutions in chloroform were spin-coated on quartz plates.

TGA and DSC measurements.

Thermogravimetric analysis (TGA) and differential Scanning calorimetry (DSC) was conducted on a METTLER-TOLEDO STARe at a heating rate of 10 °C min^{-1} and under a N_2 rate of 90 mL min^{-1}.

Electrochemical characterizations.

Cyclic voltammetry was performed on a Zahner IM6e electrochemical workstation with a three-electrode system in a solution of 0.1 M $[Bu_4N]PF_6$ acetonitrile solution at a scan rate of 100 mVs^{-1}. A glassy carbon disc coated with a small-molecule film was used as the working electrode. A Pt wire was used as the counter electrode, and Ag/Ag^+ was used as the reference electrode. A ferrocene/ferrocenium redox couple was used as the external standard, and its redox potential was 0.12 V versus Ag/Ag^+. The HOMO and LUMO energy levels were calculated from the onset of the oxidation and reduction potential of the polymer using the following equations: HOMO = -e (φ_{ox} + 4.68) (eV); LUMO = -e (φ_{red} + 4.68) (eV).

TEM and AFM measurements.

The morphologies of the polymer/acceptor blend films were investigated by AFM (Bruker, Multimode 8 SPM System) in contact under normal air conditions at room temperature with a 2 μm scanner. Samples for the TEM measurements were prepared as follows: the active layer films were spin-cast on PEDOT:PSS substrates, and the substrates with active layers were submerged in deionized water to make the active layers float onto the air-water interface. Then, the floated films were picked up on an unsupported 200 mesh copper grid for the TEM measurements. TEM measurements were performed in an FEI Tecnai G2 F20 S-Twin.

3. Solar cell fabrication and characterization

The device was fabricated with a conventional architecture of glass/indium-tin-oxide (ITO)/ poly(3,4-ethylenedioxythiophene): poly(4-styrene sulfonate) PEDOT:PSS/active layer/PDINO/Al. The ITO-coated glass was precleaned and modified by a thin layer of PEDOT:PSS, which was spin-cast from a PEDOT:PSS aqueous solution (Baytron PVP Al4083 from H.C. Stark) at 5000 rpm for 40 s and then dried at 150 °C for 15 min in air. The thickness of the PEDOT:PSS layer is 30 nm. Then, the devices were transferred to a nitrogen-filled glove box, where the active layer was spin-coated from chlorobenzene solution onto the PEDOT:PSS layer. PDINO, which serves as the electron-transport layer, is spin-coated onto the active layer at 3000 rpm for 30 s. Finally, the top 100 nm of the Al electrode was deposited in a vacuum onto the PDINO layer at a pressure of 3.0×10^{-4} Pa. The active area defined by a shadow mask is 0.056 cm^2. The current density-voltage (*J-V*) measurement of the OSCs was measured under an illumination of AM 1.5G (100 mW cm^{-2}) using an SS-F5-3A solar simulator (AAA grade, 50×50 mm^2 photobeam size) from Enli Technology Co., Ltd.). The EQE was measured by using a Solar Cell Spectral Response Measurement System QE-R3011 (Enli Technology Co., Ltd.). The light intensity at each wavelength was calibrated by a standard single-crystal Si solar cell. The PSCs were optimized by tuning the donor:acceptor (D:A) weight ratio, changing the solvent additive, and using different thermal annealing temperatures to obtain the best photovoltaic performance (as shown in Table S3-S4). The optimal D/A weight ratio is 1:1.2 (w/w) for all three OSCs. The optimal treatment conditions are 0.25% (v/v) CN and thermal annealing at 95 °C for 10 min for the DPT-T- and DPP-T-based devices, 0.25% (v/v) CN and thermal annealing at 115 °C for 10 min for the DPT-TT-based device. The optimal thickness of active layer is 100~110 nm.

Mobility measurement.

Devices with a structure of glass/ITO/PEDOT:PSS/active layer/MoO_3/Al and a structure of glass/ITO/ZnO/active layer/PDINO/Al were fabricated to measure the hole and electron mobilities, respectively. The ZnO buffer layer (thickness of 20 nm)

was deposited atop the active layer from the mixed methanol:chloroform:n-butyl alcohol (1:1:14) solution of ZnO nanoparticles at a concentration of 10 mg/mL with 4000 rpm for 30 s. The fabrication of the devices is the same as that of photovoltaic devices as described above. The device characteristics were extracted by modelling the dark current under forward bias using the space-charge-limited current expression described by the original Mott-Gurney equation:

$$J = \frac{9}{8}\varepsilon_r\varepsilon_0\mu\frac{V^2}{L^3}$$

where $\varepsilon_r \approx 3$ is the average dielectric constant of the polymer blend, ε_0 is the permittivity of the free space, μ is the charge carrier mobility, V is the applied voltage, and L is the thickness of the film.

Density functional theory (DFT) study

To investigate the fundamental aspects of DPT-T, DPT-TT, and DPP-T, density functional theory (DFT) calculations were performed based on the B3LYP/6-31G(d,p) system with the alkyl side chains substituted with methyl groups to simplify the calculations. As illustrated in Fig. S4, the three AFR acceptors exhibit relatively good planarity, with DPP-T demonstrating a more planar configuration (an N-C-C-N dihedral angle of 8.19°) compared to DPT-T (9.37°) and DPT-TT (9.88°). The HOMO/LUMO energy levels obtained from the DFT calculations for DPT-T (−5.96/−3.91 eV), DPT-TT (−5.72/−3.78 eV), and DPP-T (−5.89/−3.87 eV) are consistent with those extracted from CV measurements. The above results demonstrate that the molecular configuration, crystallinity and stacking behavior, and physicochemical properties of all-fused-ring acceptors could be significantly influenced by the different molecular extension directions.

Charge recombination dynamics and carrier lifetime and charge extraction time study

The dependence of J_{sc} on the light intensity (P_{light}) was analysed to evaluate the charge recombination kinetics of the OSCs by using the equation: $J_{sc} \propto P_{light}^{\alpha}$, where the power-law exponential factor α can indicate the degree of bimolecular recombination.[3] As shown in Fig. S8a, α values of 0.990, 0.991, and 0.905 were fitted for DPT-T-, DPT-TT-, and DPP-T-based devices, respectively, suggesting the weakest bimolecular recombination in the DPT-TT-based device. Additionally, the trap-assisted recombination of the devices was studied by plotting the V_{oc} values versus P_{light}: $V_{oc} \propto n\left(\frac{kT}{q}\right) \ln P_{light}$, where k is the Boltzmann constant, T is the absolute temperature, and q is the elementary charge. In comparison with the devices based on DPT-T and DPP-T with slopes of 1.15 and 0.92 kT/q, the DPT-TT-based device exhibited a slope closer to 1 kT/q (1.06 kT/q), as fitted in Fig. S8b, referring to the lower degree of weaker trap-assisted recombination.[4] Subsequently, the dynamics of charge carriers in the devices were evaluated through transient photocurrent (TPC) and transient photovoltage (TPV) measurements.[5] As depicted in Fig. S8c, relative to the DPT-T- and DPP-T-based devices with charge extraction times of 0.48 and 0.55 μs, respectively, the DPT-TT-based device exhibited a reduced charge extraction time of 0.20 μs. Additionally, the DPT-TT-based device demonstrated an extended carrier lifetime of 1.10 μs compared to the other two devices (Fig. S8d). The above comprehensive analysis shows that DPT-TT-based devices exhibit enhanced charge transport properties, improved charge dissociation and extraction efficiency, reduced bimolecular and trap-assisted recombination, and prolonged carrier lifetime, substantiating the superior J_{sc} and FF observed in J-V measurements.

Contact angle measurements study

Contact angle measurement of films was performed to gain a deeper understanding of the diverse orientations of extended conjugation on the morphology of active layers. As shown in Fig. S10 and Table S5 in the Supporting Information, the surface tension (γ) values for PTQ10, **DPT-T**, **DPT-TT**, and **DPP-T** were 21.5, 24.6, 26.0, and 24.0

mN m^{-1}, respectively, on the basis of Wu's model. Subsequently, the miscibility of the blends was estimated by calculating the Flory–Huggins interaction parameter χ, which was determined through the following equation:[6-8]

$$\chi = K\left(\sqrt{\gamma_a} - \sqrt{\gamma_d}\right)^2$$

where K is a constant and γ_a and γ_d are the surface energies of the acceptor and donor, respectively.[9] The calculated χ values for PTQ10:**DPT-T**, PTQ10:**DPT-TT**, and PTQ10:**DPP-T** were 0.10 K, 0.21 K, and 0.07 K, respectively. The larger χ value between PTQ10 and **DPT-TT** associated with the stronger crystallinity compared to DPT-T and DPP-T contributes to the well-develop morphology properties.

4. Supplementary Figures and tables

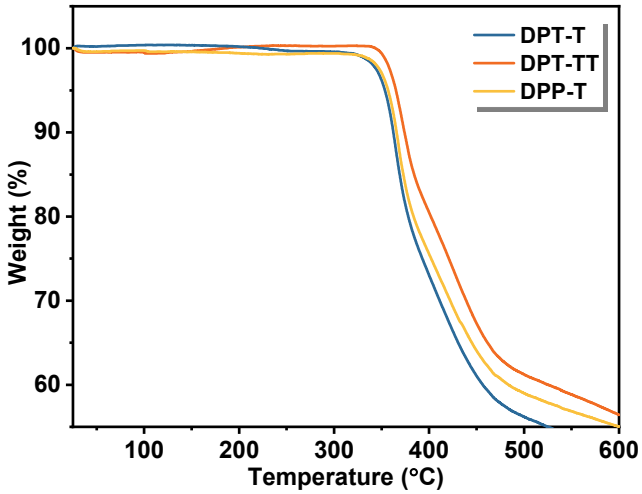

Fig. S1 TGA curve of DPT-T, DPT-TT, DPP-T under N_2 atmosphere at a scan rate of 10 °C min^{-1}. The T_d of DPT-T, DPT-TT, and DPP-T are 353.5 °C, 365 °C, and 357 °C, respectively.

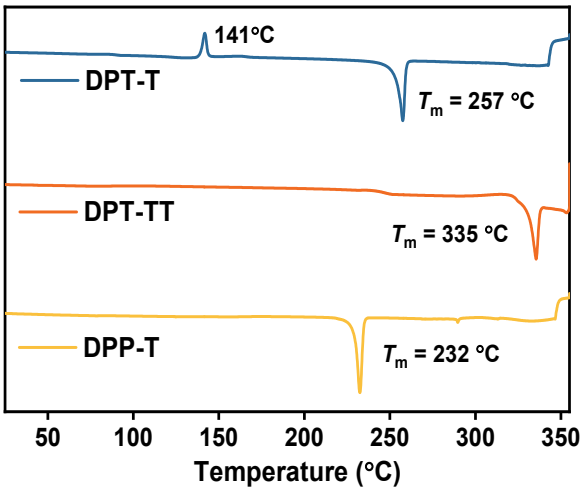

Fig. S2 DSC second heating of DPT-T, DPT-TT, and DPP-T under N_2 atmosphere at a scan rate of 10 °C min^{-1}.

Table S1 Calculated measured XRD data.

Materials	Lamellar stacking		π-π stacking	
	Location (degree)	*d*-spacing (Å)	Location (degree)	*d*-spacing (Å)
DPT-T	5.27	16.74	24.21	3.70
DPT-TT	6.65	13.28	25.52	3.48
DPP-T	6.74	13.10	24.06	3.70

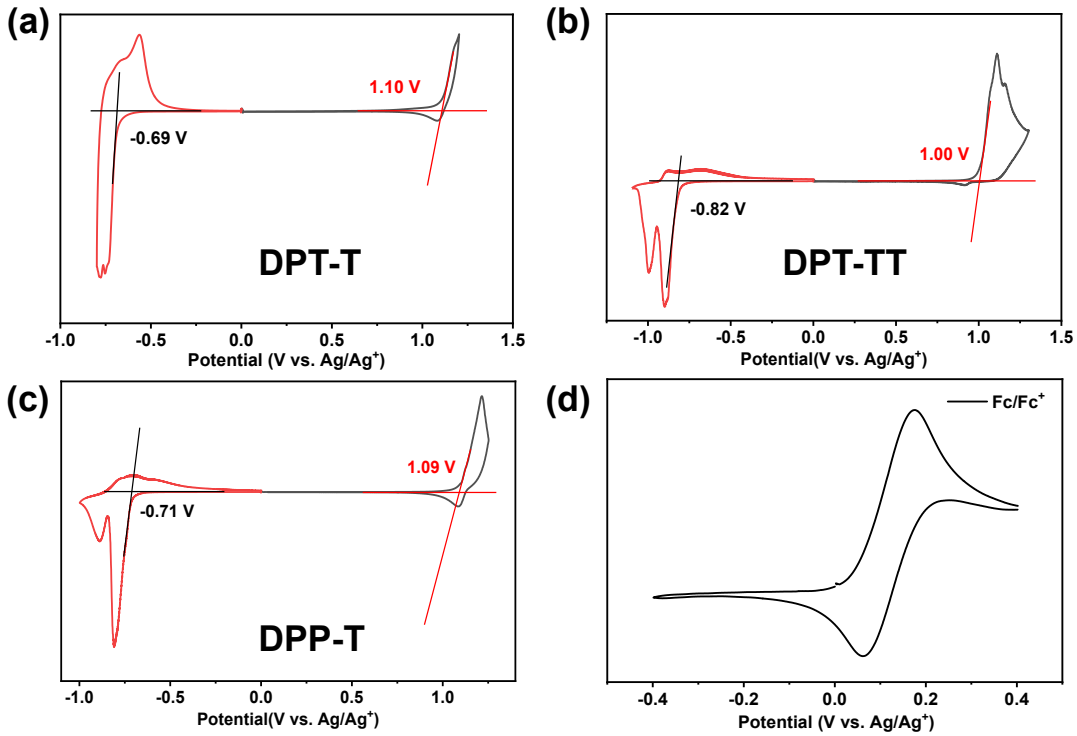

Fig. S3 Cyclic voltammograms of (a) DPT-T, (b) DPT-TT, (c) DPP-T and (d) ferrocene.

Fig. S4 Optimized molecular conformations and frontier molecular orbital surfaces of DPT-T, DPT-TT and DPP-T.

Table S2. Physicochemical properties of DPT-T, DPT-TT, and DPP-T.

Acceptor	λ_{max} [nm]		λ_{onset} [nm]	E_g [eV]	Absorption coefficient ($\times 10^4$ cm^{-1})	HOMO [eV]	LUMO [eV]
	Solution	Film					
DPT-T	704	765	857	1.44	7.76	−5.79	−3.99
DPT-TT	737	817	905	1.37	9.13	−5.68	−3.86
DPP-T	715	765	860	1.44	6.68	−5.77	−3.96

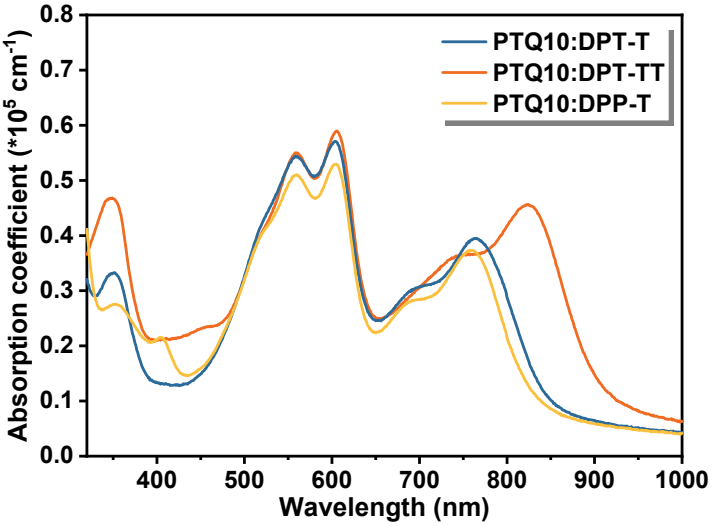

Fig. S5 UV–vis absorption spectra of the blend films of PTQ10:DPT-T, PTQ10:DPT-TT, and PTQ10:DPP-T.

Table S3 Photovoltaic performance of solar cells based on different donors under illumination of AM 1.5 G, 100 mW cm^{-2}.

Active layer	D:A	V_{oc} (V)	J_{sc} (mA cm^{-2})	FF (%)	PCE (%)
PM6:DPT-TT	1:1.2	0.714	22.33	59.6	9.51
	1:1.4	0.709	22.11	55.7	8.74
	1:1.6	0.715	21.81	56.7	8.86
	1:0.8	0.752	16.79	43.2	5.46

	1:1	0.750	18.54	57.7	8.03
	1:1.2	0.747	20.74	61.1	9.46
	1:1.4	0.734	21.89	53.8	8.65
	1:1.6	0.755	21.09	56.9	9.05

Table S4 Photovoltaic performance of solar cells based on PTQ10:DPT-T, PTQ10:DPT-TT and PTQ10:DPP-T blend films with different optimization conditions under the illumination of AM 1.5 G at 100 mW cm^{-2}.

Active layer	TA temperature	Additive	V_{oc} (V)	J_{sc} (mA cm^{-2})	FF (%)	PCE (%)
PTQ10:DPT-T	/	/	0.697	18.56	55.2	7.15
		0.25% CN	0.697	19.05	63.0	8.37
	95 °C	/	0.699	19.89	69.2	9.63
		0.25% CN	0.697	19.82	70.3	9.71
	115 °C	/	0.694	19.82	69.0	9.50
		0.25% CN	0.687	20.17	69.1	9.58
PTQ10:DPT-TT	/	/	0.747	20.74	61.1	9.46
		0.25% CN	0.735	22.38	67.5	11.10
	95 °C	/	0.716	24.26	66.6	11.58
		0.25% CN	0.716	23.74	71.2	12.12
	115 °C	/	0.715	24.79	67.5	11.97
		0.25% CN	0.707	24.15	71.1	12.14
PTQ10:DPP-T	/	/	0.748	16.66	49.5	6.46
		0.25% CN	0.740	16.38	42.7	5.18

95 °C	/	0.732	17.80	49.5	6.46
	0.25% CN	0.730	17.96	50.2	6.58
115 °C	/	0.724	16.77	46.1	5.60
	0.25% CN	0.726	17.34	47.8	6.02

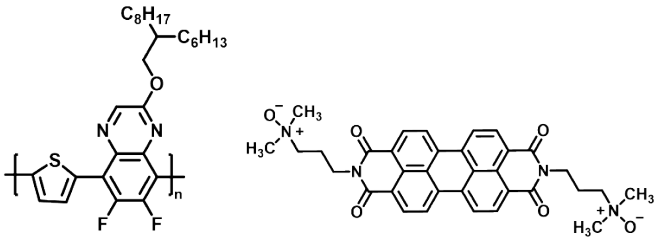

Fig. S6 The chemical structures of PTQ10 and PDINO.

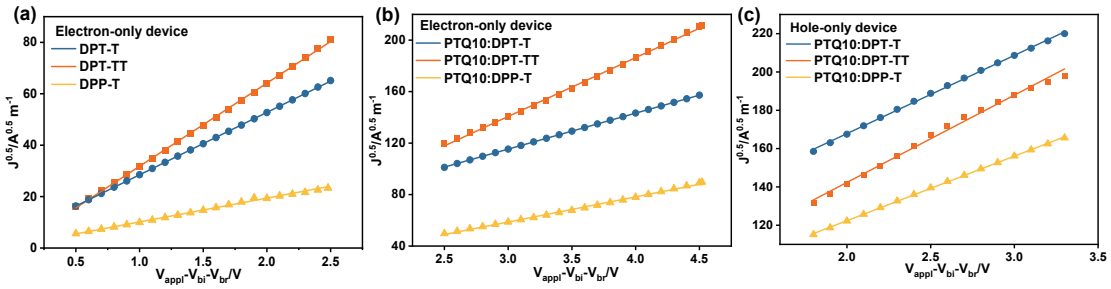

Fig. S7 $J^{0.5}$-V plots of (a) the electron-only devices of the DPT-T, DPT-TT, and DPP-T neat films. $J^{0.5}$-V plots of (b) the electron-only and (c) hole-only devices of PTQ10:DPT-T, PTQ10:DPT-TT, and PTQ10:DPP-T blend films.

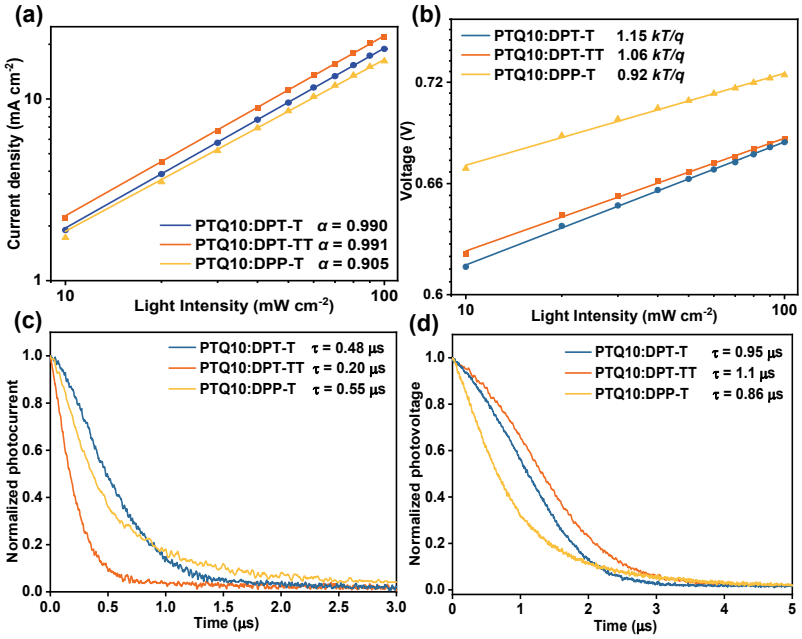

Fig. S8 (a) Dependence of J_{sc} on the light intensity, (b) dependence of V_{oc} on the light intensity, (c) Transient photocurrent profiles, and (d) transient photovoltage profiles of the optimal OSCs based on PTQ10:DPT-T, PTQ10:DPT-TT, and PTQ10:DPP-T

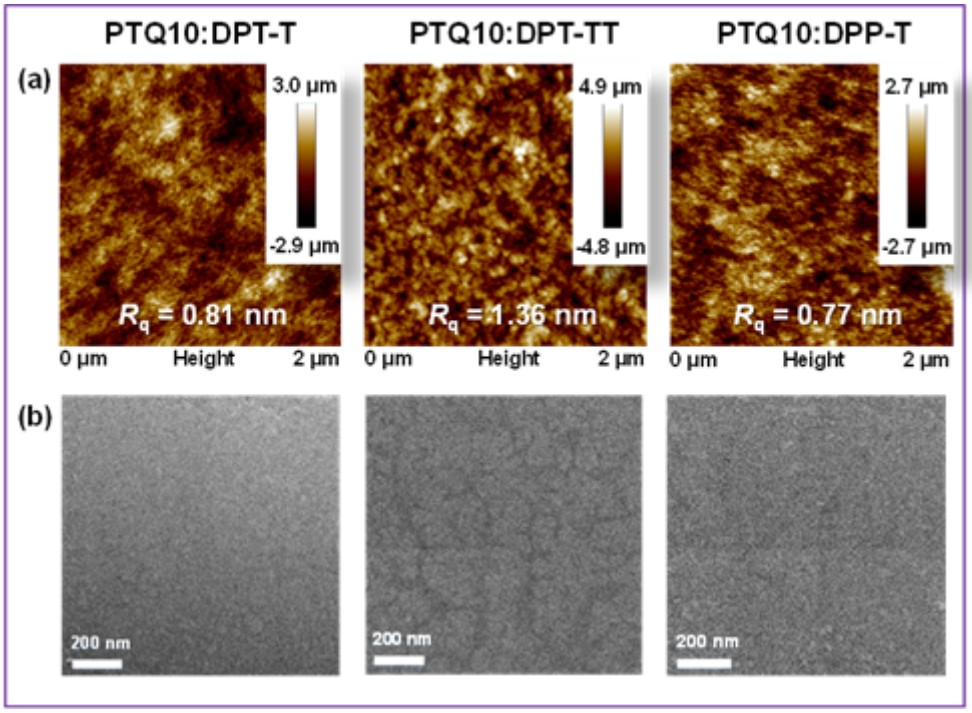

Fig. S9 (a) AFM height images and (b) TEM images of the optimal PTQ10:DPT-T, PTQ10:DPT-TT, and PTQ10:DPP-T blend films.

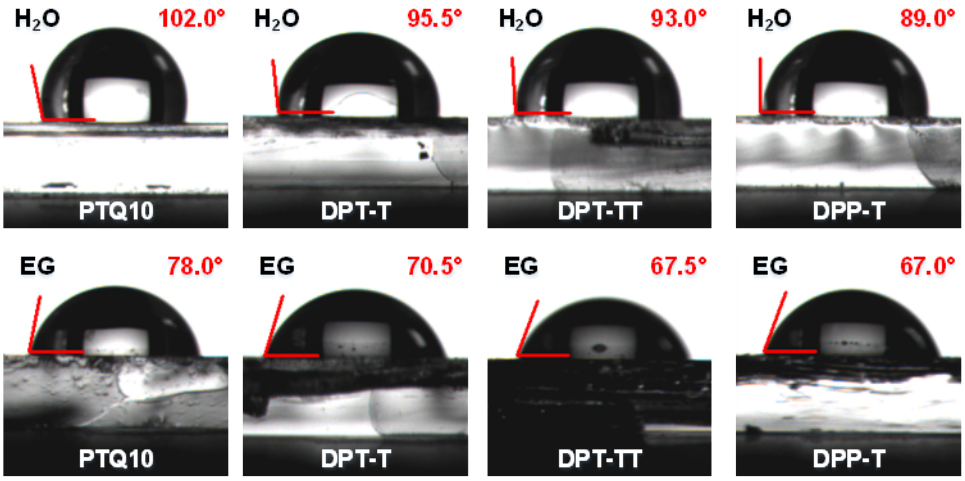

Fig. S10 Contact angle measurement images of the neat films of PTQ10, DPT-T, DPT-TT, and DPP-T by using water and ethylene glycol liquid drops.

Table S5 Surface tension energy and the Flory−Huggins interaction parameter of neat and blend films.

Material	γ^d (mN m^{-1})	γ^p (mN m^{-1})	γ (mN m^{-1})	χ with PTQ10 ($\times$ K mN m^{-1})
PTQ10	20.35	1.18	21.53	/
DPT-T	22.34	2.30	24.64	0.10
DPT-TT	23.14	2.84	25.97	0.21
DPP-T	18.33	5.69	24.02	0.07

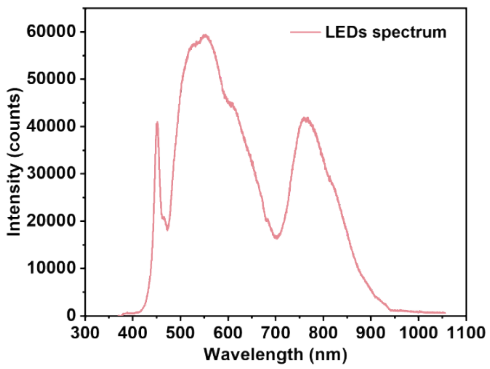

Fig. S11 The spectrum of LEDs.

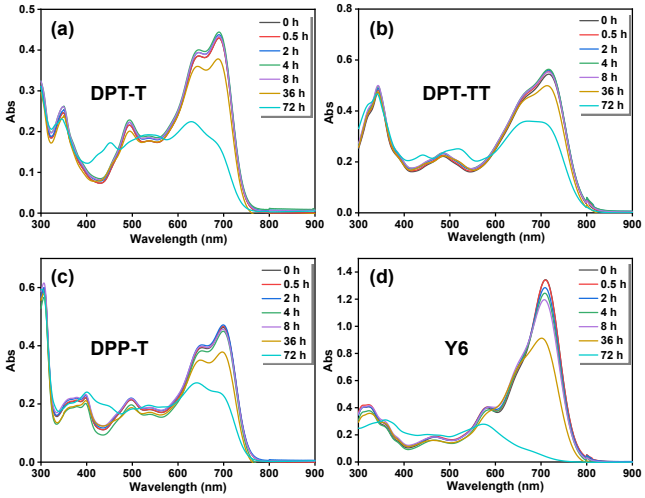

Fig. S12 UV–Vis absorption spectra of (a) DPT-T, (b) DPT-TT, (c) DPP-T, and (d) Y6 under different irradiation times (100 mW cm^{-2} AM 1.5 G) in THF. The concentration of NFAs is controlled at 10^{-5} M.

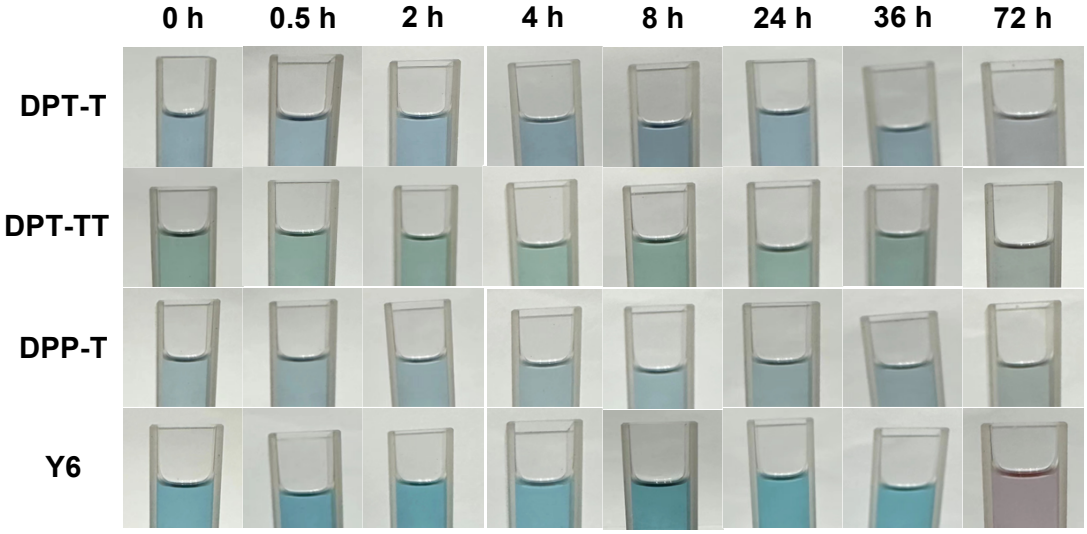

Fig. S13 The color variation of DPT-T, DPT-TT, DPP-T, and Y6 for different irradiation times in THF solutions (10^{-5} M).

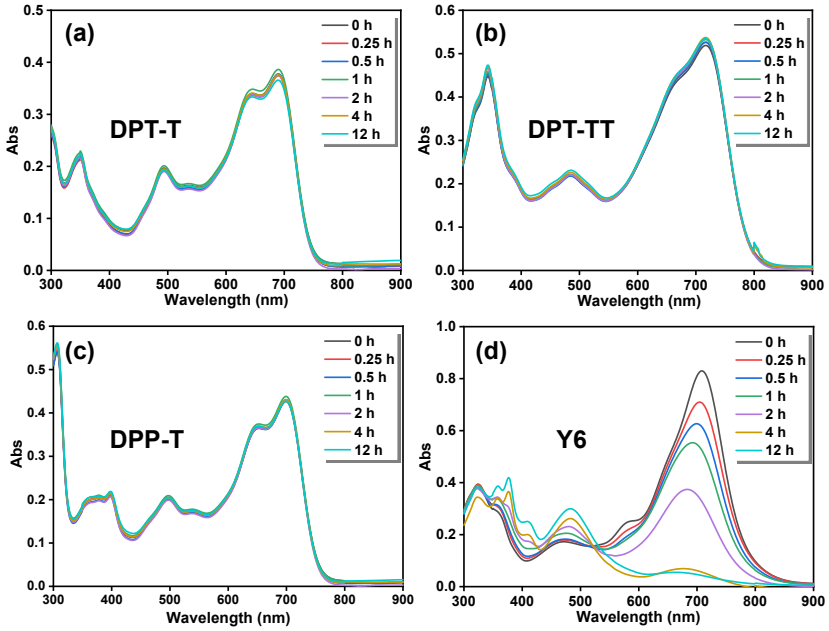

Fig. S14 The UV–vis absorption spectra of (a) DPT-T, (b) DPT-TT, (c) DPP-T and (d) Y6 treated in diluted THF solution (10^{-5} M) with 100 equiv of ethanolamine at different times.

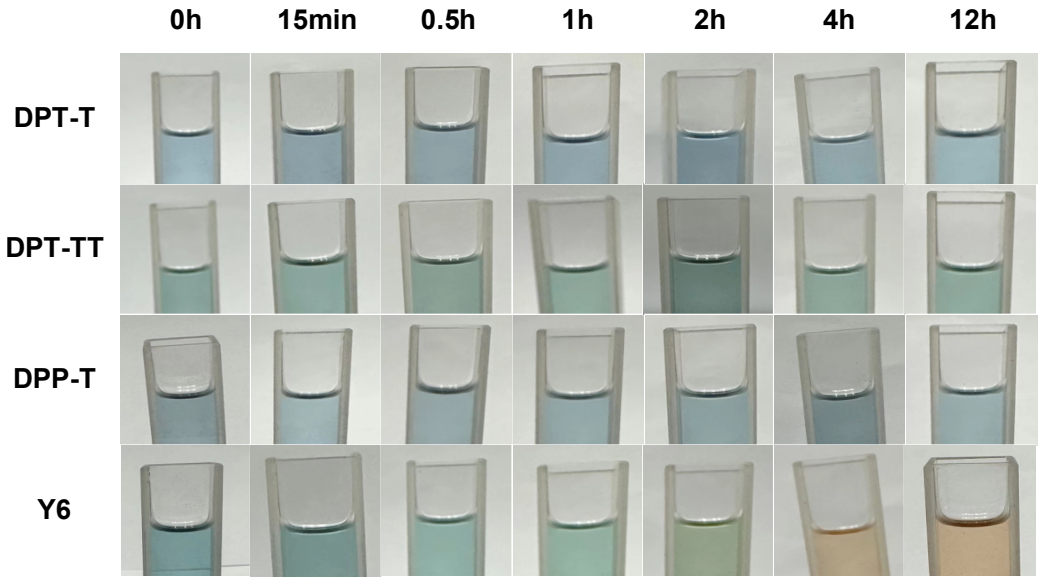

Fig. S15 The color variation of DPT-T, DPT-TT, DPP-T, and Y6 treated in the diluted THF solution (10^{-5} M) with 100 equiv ethanolamine for different times.

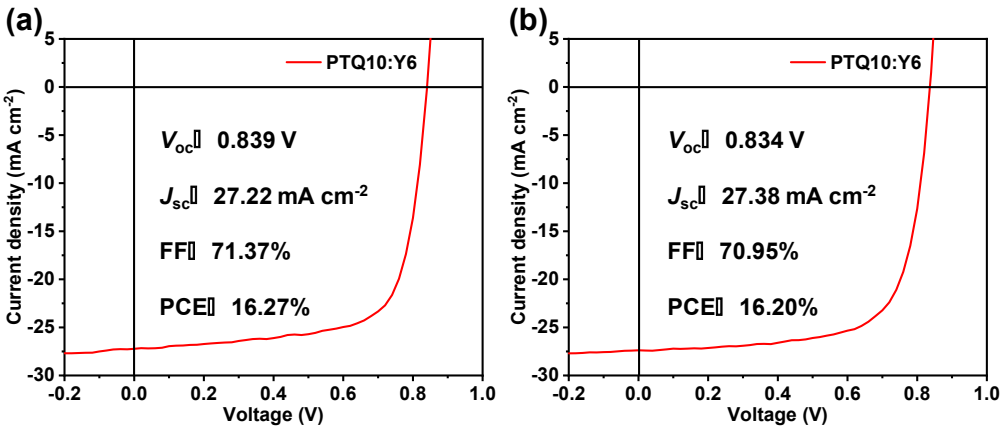

Fig. S16 The initial *J-V* curve and the corresponding key photovoltaic parameters of PTQ10:Y6-base device of (a) illumination and (b) thermal stability.

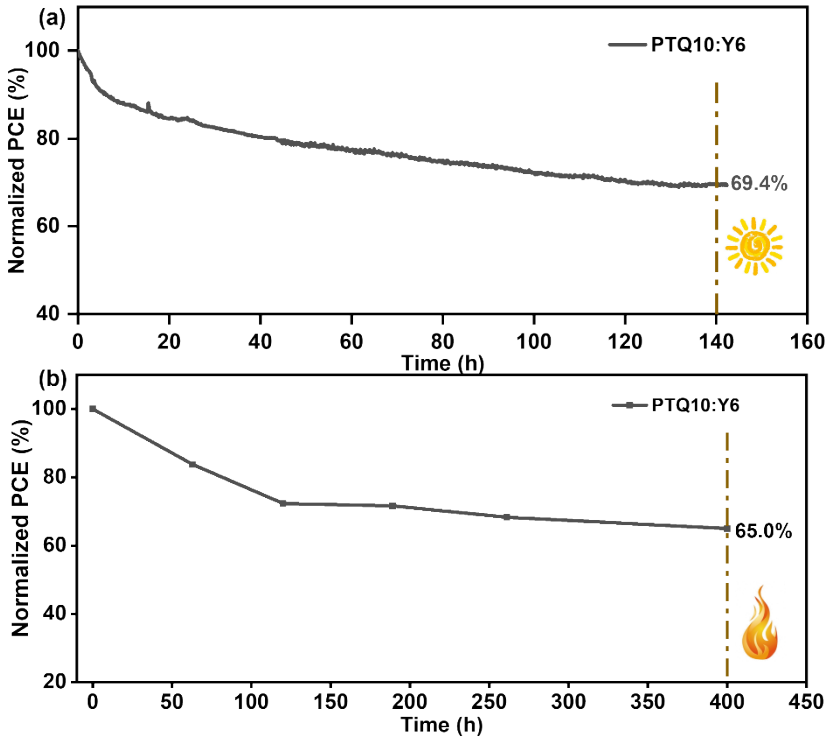

Fig. S17 (a) Normalized PCE of inverted OSC devices based on PTQ10:Y6 under AM 1.5 G illumination at 100 mW cm^{-2} from white LEDs in a nitrogen-filled glovebox. The device decayed to 69.4% of its initial PCE (PCE = 16.27%) after 140 h of illumination. (b) Normalized PCE of inverted OSC devices based on PTQ10:Y6 under thermal aging at 65 °C in a nitrogen-filled glovebox. The device exhibited inferior thermal stability, experiencing an approximately 35.0% decrease in initial efficiency (PCE = 16.20%) after 400 h.

and (b) under thermal aging at 65 °C in a nitrogen-filled glovebox.

, while

Fig. S18 Absorption spectra of DPT-T, DPT-TT, DPP-T, and Y6 film with the increasing thermal annealing temperature.

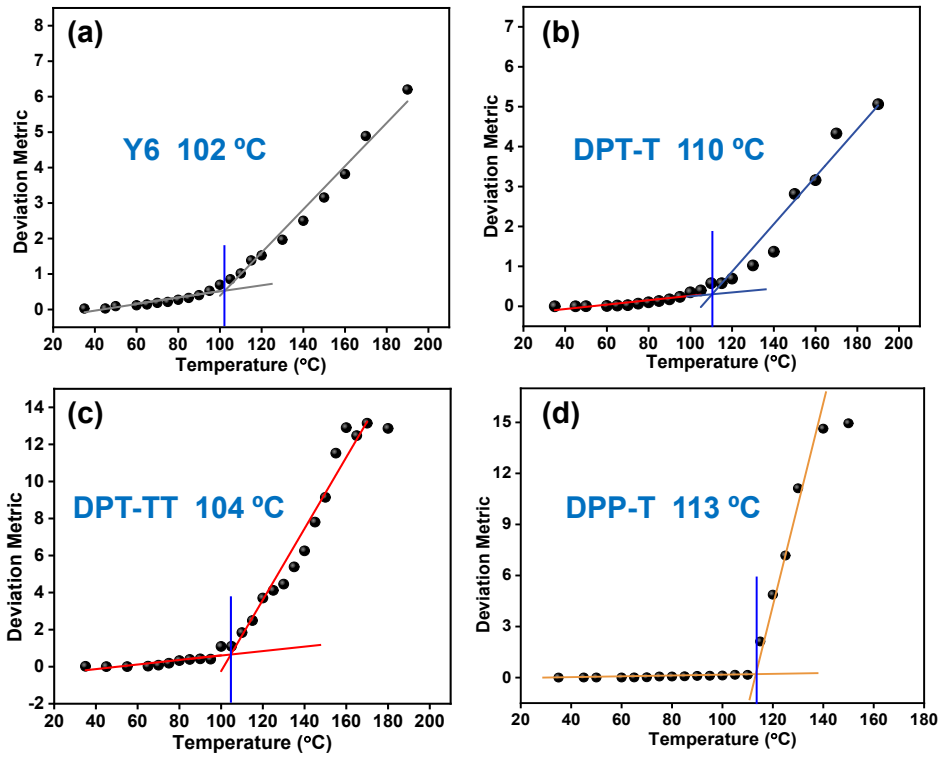

Fig. S19 Plots of the deviation metric of (a) Y6, (b) DPT-T, (c) DPT-TT, and (d) DPP-T films as a function of annealing temperature.

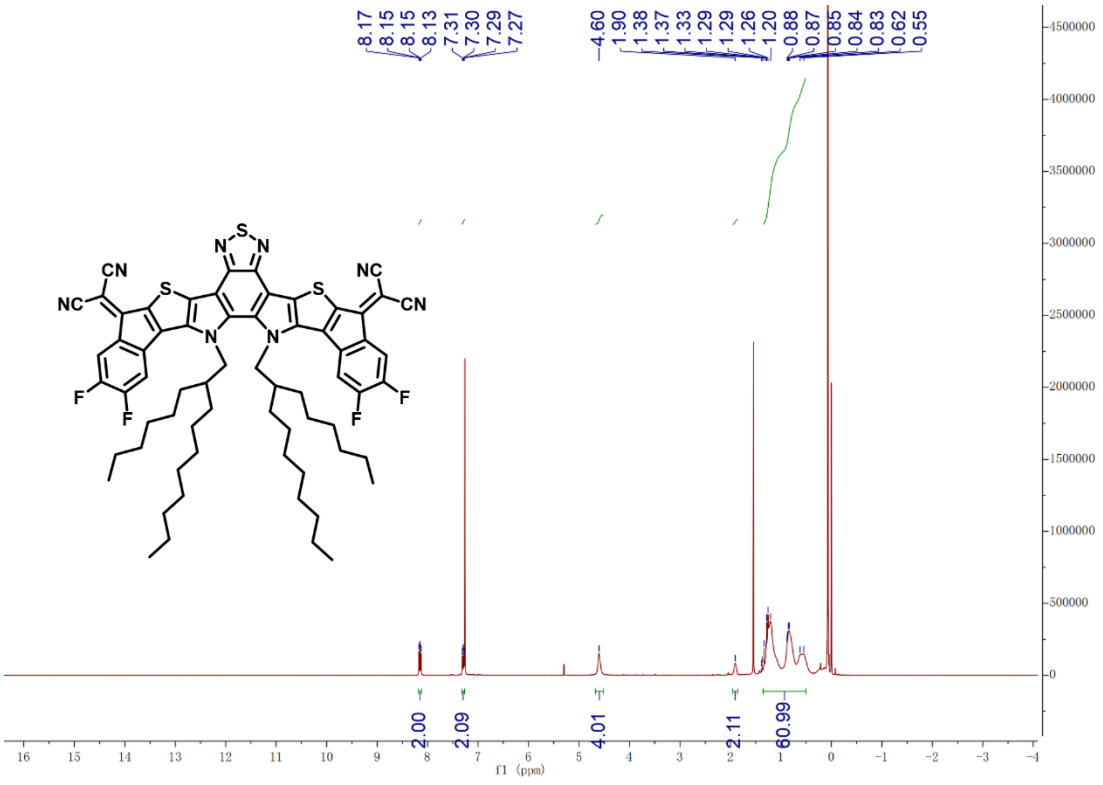

Fig. S20 The ^{1}H NMR of **DPT-T**.

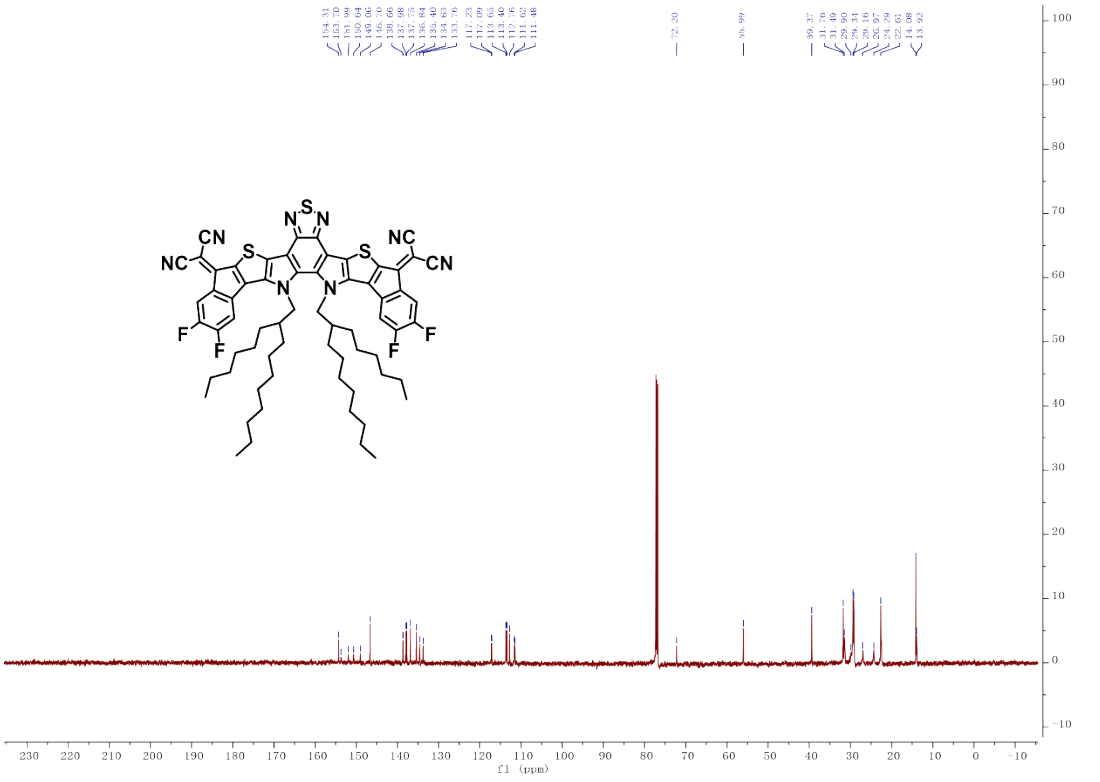

Fig. S21 The ^{13}C NMR of **DPT-T**.

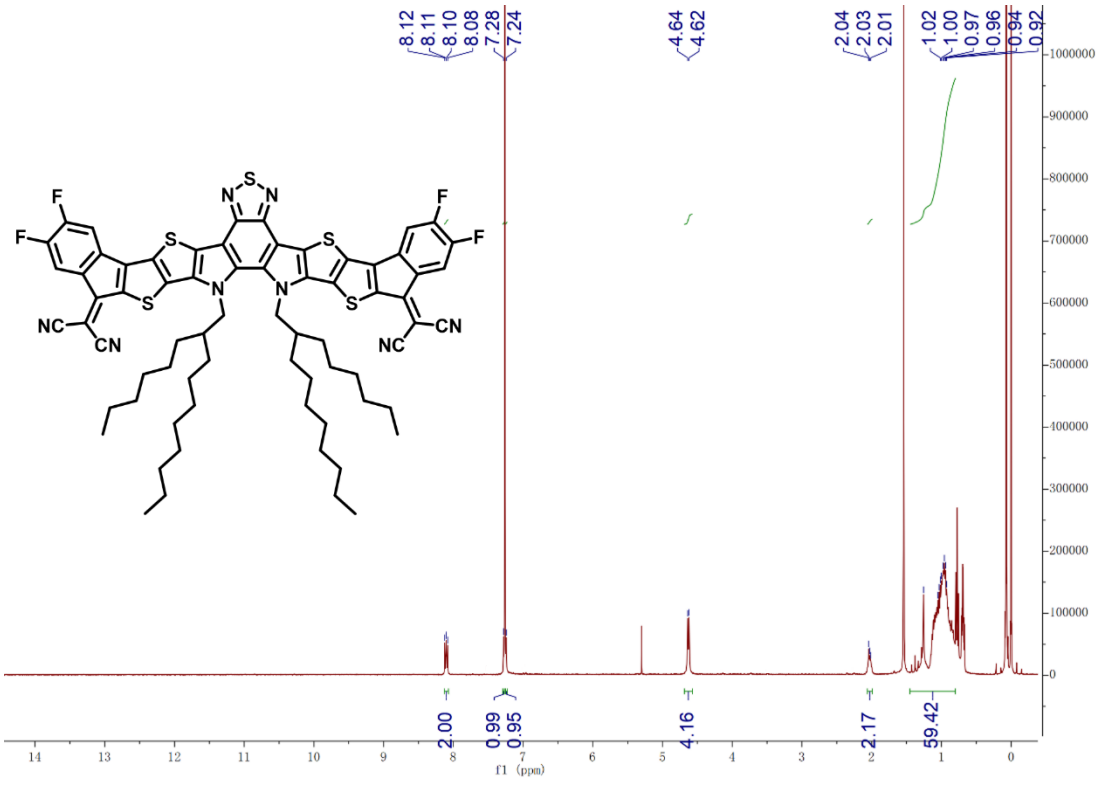

Fig. S22 The ^{1}H NMR of **DPT-TT**.

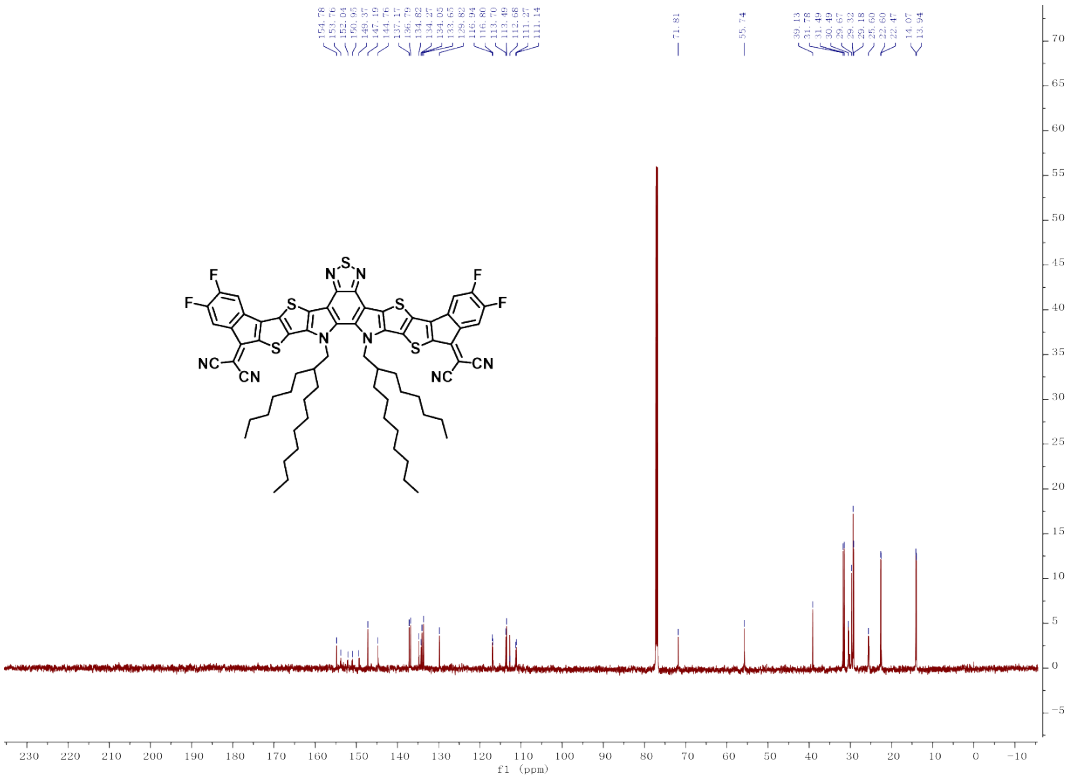

Fig. S23 The ^{13}C NMR of **DPT-TT**.

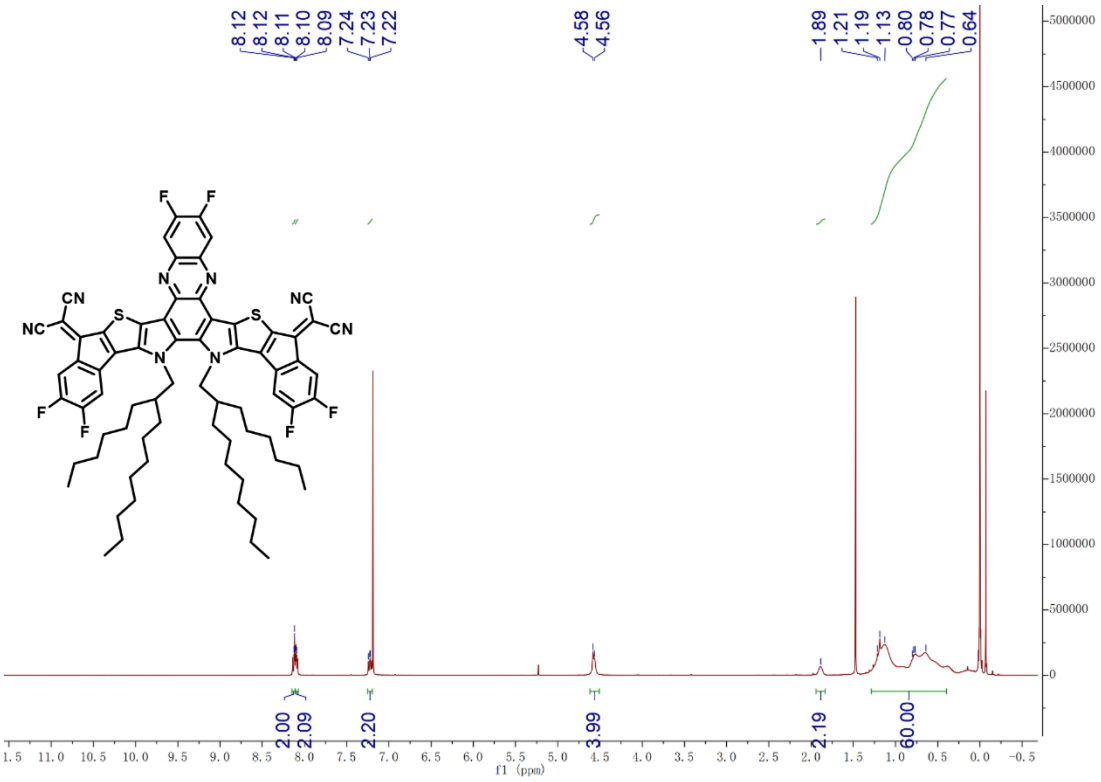

Fig. S24 The ^{1}H NMR of **DPP-T**.

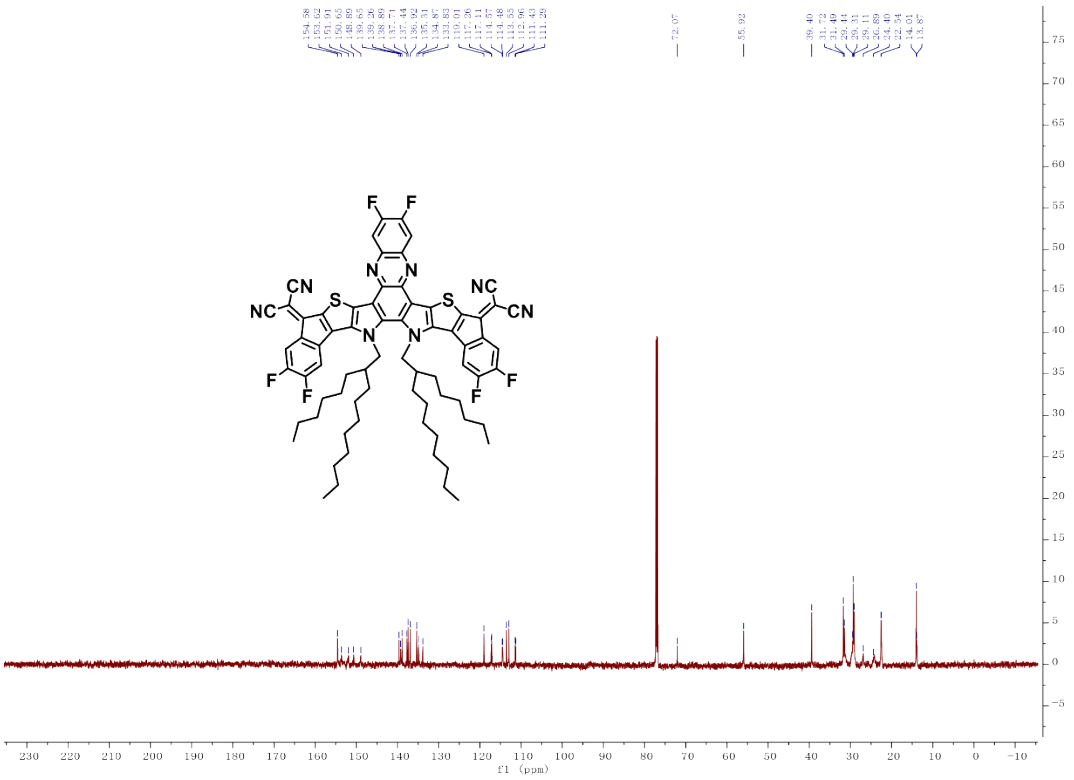

Fig. S25 The ^{13}C NMR of **DPP-T**.

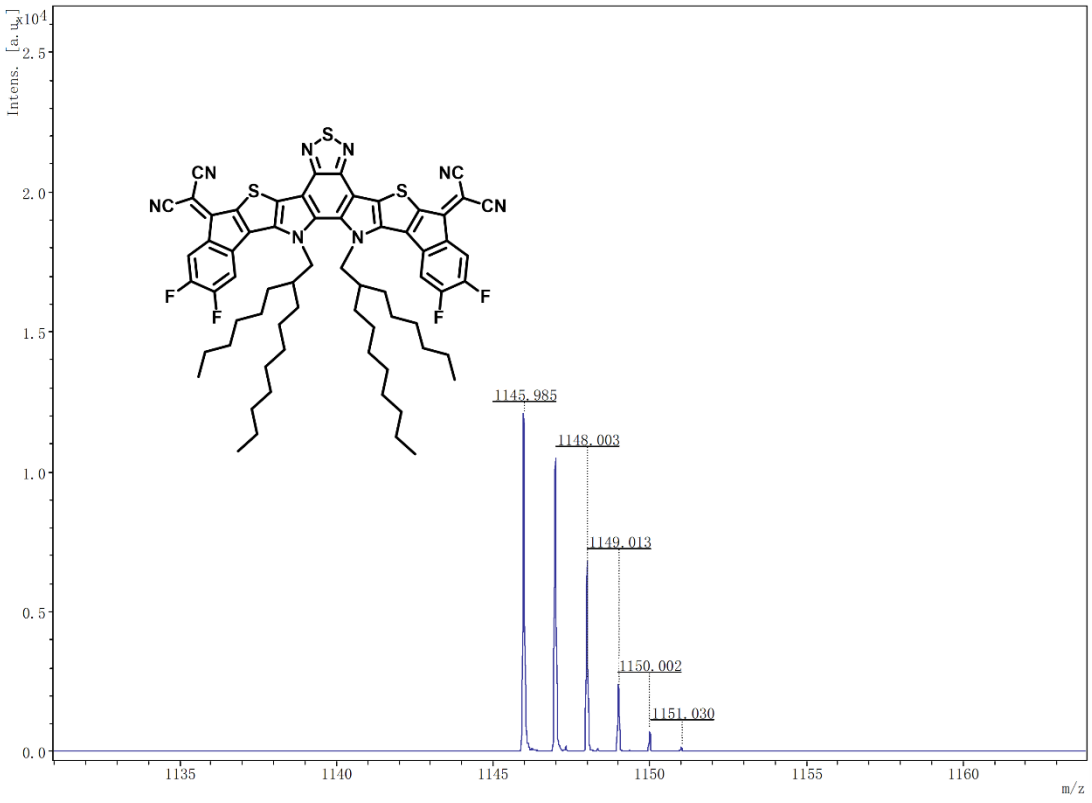

Fig. S26 Mass spectrum of **DPT-T**.

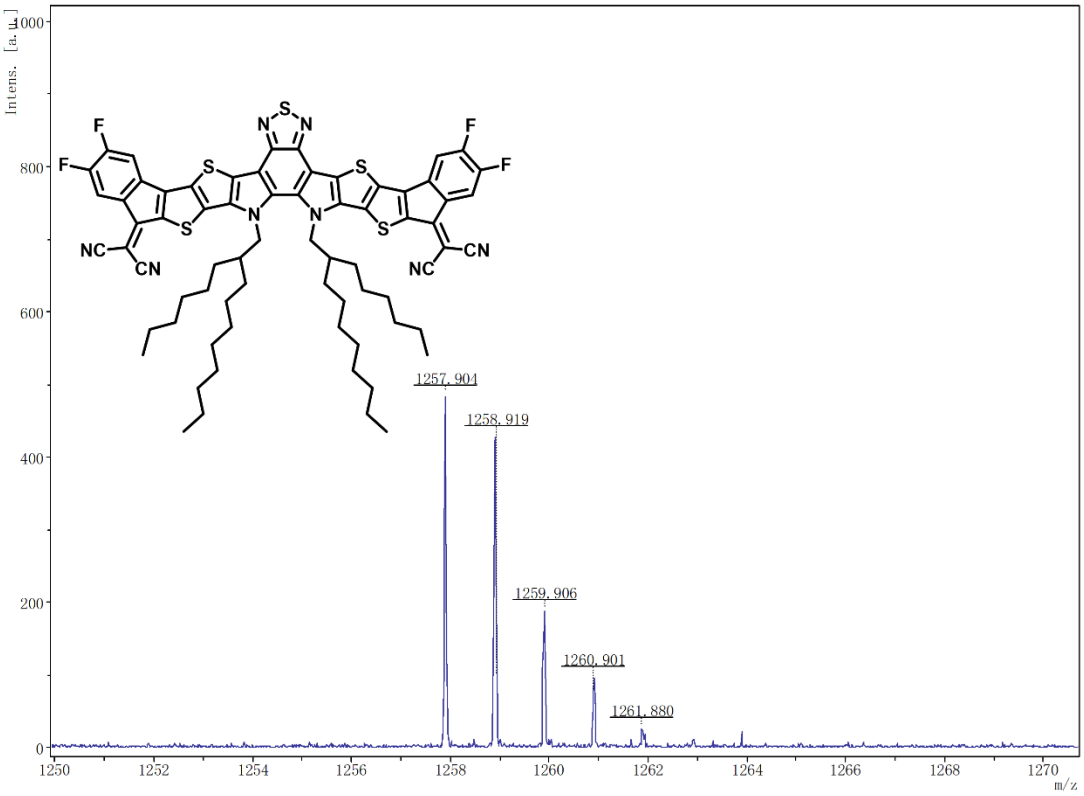

Fig. S27 Mass spectrum of **DPT-TT**.

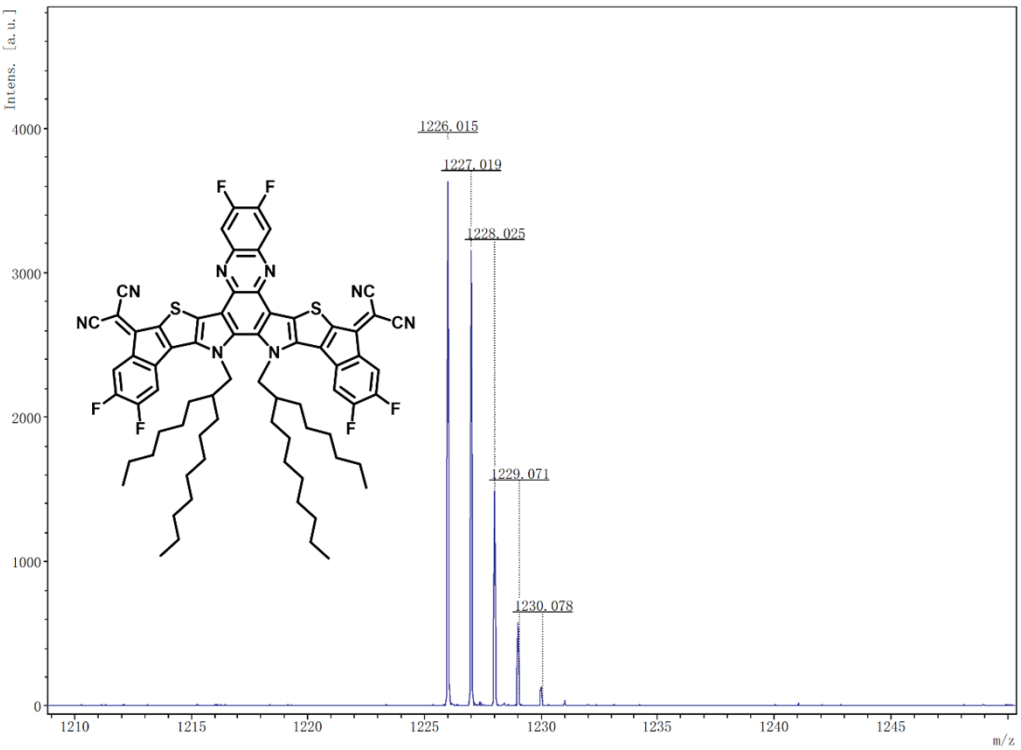

Fig. S28 Mass spectrum of **DPP-T**.

Reference

1. C. Sun, F. Pan, H. Bin, J. Zhang, L. Xue, B. Qiu, Z. Wei, Z.-G. Zhang and Y. Li, *Nat. Commun.*, 2018, **9**, 743.
2. W. Liu, S. Xu, H. Lai, W. Liu, F. He and X. Zhu, *CCS Chemistry*, 2023, **5**, 654-668.
3. P. Schilinsky, C. Waldauf and C. J. Brabec, *Applied Physics Letters*, 2002, **81**, 3885-3887.
4. L. J. A. Koster, V. D. Mihailetchi, R. Ramaker and P. W. M. Blom, *Appl. Phys. Lett.*, 2005, **86**, 123509.
5. H. Yang, S. Bao, N. Cui, H. Fan, K. Hu, C. Cui and Y. Li, *Angew. Chem. Int. Ed.*, 2022, **62**, e202216338.
6. S. Kouijzer, J. J. Michels, M. van den Berg, V. S. Gevaerts, M. Turbiez, M. M. Wienk, R. A. Janssen, *J. Am. Chem. Soc,* 2013, **135**, 12057
7. J. Zhang, C. H. Tan, K. Zhang, T. Jia, Y. Cui, W. Deng, X. Liao, H. Wu, Q. Xu, F. Huang, Y. Cao, *Adv. Energy Mater*, 2021, **11**, 2102559.
8. D. Zhou, C. Liao, S. Peng, X. Xu, Y. Guo, J. Xia, H. Meng, L. Yu, R. Li, Q. Peng, *Adv. Sci*, 2022, **9**, 2202022.
9. Z. Zhang, Z. Li, P. Wang, H. Chen, K. Ma, Y. Zhang, T. Duan, C. Li, Z. Yao, B. Kan, X. Wan and Y. Chen, *Adv. Funct. Mater.*, 2023, **33**, 2214248.